Pergamon

Int. J. Heat Mass Transfer. Vol. 41, Nos 8–9, pp. 1035–1048, 1998

Printed in Great Britain
0017–9310/98 $19.00+0.00

PII: S0017–9310(97)00197–X

A continuum model for the transport of heat, mass and momentum in a deformable, multicomponent mush, undergoing solid–liquid phase change

M. D. JACKSON and M. J. CHEADLE

Department of Earth Sciences, University of Liverpool, Jane Herdman Laboratories, Brownlow Street, Liverpool L69 3BX, U.K.

(*Received* 11 *February* 1997 *and in final form* 11 *June* 1997)

Abstract—Motivated by a geological problem, the continuum conservation equations governing the transport of heat, mass and momentum in a deformable multicomponent mush undergoing solid–liquid phase change are presented, and a one-dimensional (1-D) model of a layer heated from below investigated numerically. The results indicate that phase transport exercises a strong control on heat transport. The form of the spatial distribution of liquid depends upon the relative transport rates of heat and buoyant liquid; a high porosity wave may develop at the top of the mixed phase region, the amplitude of which increases with time until the contiguity of the solid matrix breaks down and a slurry forms. Phase compositions are fixed by the requirement of local thermodynamic equilibrium, and are deduced from published equilibrium phase change experiments. © 1997 Elsevier Science Ltd.

1. INTRODUCTION

Most common rock types are complex, non-eutectic, multicomponent substances which undergo solid–liquid phase change over a temperature and pressure range, leading to the formation of a mixed phase region in which solid and liquid phases coexist. Often the phases are mobile, and during phase change migrate relative to one another, resulting in their partial or complete separation; this occurs when melt segregates from a melting rock, or crystals separate from a solidifying magma. A quantitative understanding of these coupled phase change and phase transport processes is of fundamental importance in the earth sciences, because they are responsible for the origin and chemical diversity of all the igneous rocks.

Interest in binary and multicomponent phase change spans a range of scientific and engineering disciplines, including metallurgy, materials science and the earth sciences, and has motivated the development of an increasing number of quantitative transport models [1–5]. Most of these concern binary phase change systems such as metallic alloys, and have been applied to solidification processes such as casting and welding [6–8]. In contrast, few quantitative transport models of melting processes have been developed which can be applied to geological systems. Models developed for metallurgical systems can rarely be directly applied to geological systems, because of differences in the rheological properties and initial and boundary conditions of the mixed phase region [9].

When a rock composed of silicate minerals melts, the solid fraction maintains a continuous connecting matrix, termed a mush, until the liquid volume fraction exceeds a certain value, which is usually termed the 'Critical Melt Fraction' (CMF) [10, 11]. If the surface topology of the solid grains is in local thermodynamic and mechanical equilibrium, the liquid fraction collects along grain edges and may form an interconnected network, in which case the solid matrix is permeable [12–14]. Phase change models of metallurgical mushes usually assume that the matrix is rigid [3–5, 15]; in geological systems, liquid enhanced diffusional creep processes provide a mechanism for changing the morphology of the solid matrix, so that on a macroscopic scale the matrix is not rigid, and will viscously deform in response to liquid phase transport [16–18].

Previous quantitative models of liquid transport through a melting, deformable mush have decoupled the phase change and phase transport processes, and have either neglected phase change entirely, or have externally imposed the rate of phase change [19–22]. Whilst this approximation is valid for some geological systems, phase change and phase transport are usually complementary processes which cannot be decoupled. Often a mixed phase region is produced when rock is heated from below; for instance, when hot magma intrudes the lower continental crust as a horizontal layer, causing melting in the overlying rock [23, 24]. The liquid produced is usually compositionally and thermally buoyant, so a pressure gradient is present to drive liquid migration relative to the solid matrix. The system is complex because compositional gradi-

NOMENCLATURE

a	solid phase grain radius
b	constant in permeability relationship
c_p	specific heat capacity
c_{eff}	effective specific heat capacity
C	compaction rate
D	normalized difference between isotherm positions [equation (46)]
g	gravitational acceleration
$\mathbf{I}$	interphase force per unit volume
$\mathbf{k}$	thermal conductivity
k	permeability
K	characteristic permeability
$\hat{k}$	unit vector, vertical
L	specific latent heat
n	exponent in permeability relationship
P	pressure
Ste	Stefan number
t	time
T	temperature
$\mathbf{v}$	velocity vector
w	vertical component of velocity
z	vertical Cartesian coordinate.

Greek symbols

δ	characteristic lengthscale
ϕ	liquid volume fraction (porosity)
φ	equilibrium liquid volume fraction at $z = 0$
Γ	rate of production of phase
κ_{eff}	dimensionless effective thermal diffusivity
θ	equilibrium liquid volume fraction; numerically equivalent to the dimensionless temperature
μ	shear viscosity
ν	equilibrium phase volume fraction
ξ	bulk viscosity
ρ	density
$\boldsymbol{\sigma}$	stress tensor
τ	characteristic timescale
ω	characteristic velocity.

Subscripts

b	value at $z = 0$
i	pertaining to the ith isotherm
l	liquid
liq	liquidus
m	mixture
s	solid
sol	solidus.

Superscripts

l	liquid
s	solid.

ents exist in both phases, and the phases may interact and exchange components during phase transport [25].

Motivated by this geological problem, the aim of this paper is to present a model for the transport of heat, mass and momentum in a viscously deformable, multicomponent mush which is undergoing solid–liquid phase change due to heating from below. A continuum approach is adopted, because continuum formulations are well suited for modelling the transition between solid and liquid phases over a temperature and pressure interval, with associated latent heat evolution and coupled transport processes [1]. Although motivated by a geological problem, the formulation presented here may be applied to any melting, multicomponent system in which fluid migration coupled with solid deformation is an important process, and which satisfies the assumptions made in deriving the governing equations.

2. MODEL FORMULATION

Consider a homogenous, isotropic, multicomponent material which is initially at its solidus temperature T_{sol}, and which is semi-infinite in the positive z (vertical) direction. At $t = 0$ the temperature of the $z = 0$ plane is instantaneously increased to a temperature T_b which is greater than the solidus of the overlying material and is, subsequently, maintained at this temperature for all time (Fig. 1). Solid–liquid phase change in the material leads to the formation of a mushy mixed phase region adjacent to the $z = 0$ plane. The liquid phase produced is buoyant and interconnected; the solid phase can viscously deform in response to liquid phase transport. Liquid and solid phases are assumed always to be in local thermodynamic equilibrium.

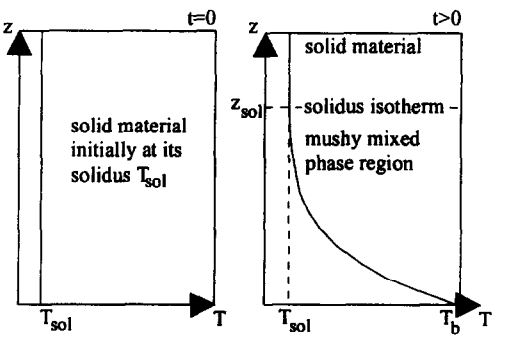

Fig. 1. The development of a mushy mixed phase region due to heating from below.

2.1. *Conservation equations*

The equations governing conservation of mass, energy and momentum in the mixed phase region are presented in Cartesian coordinates throughout, with z positive upwards. Assuming there are no void spaces or other phases present in the mixed phase region, the statement of conservation of mass of the liquid and solid phases may be expressed in terms of the liquid volume fraction (porosity) ϕ as [1–5, 19–22]

$$\frac{\partial}{\partial t}(\rho_l\phi)+\nabla\cdot(\rho_l\phi\mathbf{v}_l)=\Gamma_l \tag{1}$$

$$\frac{\partial}{\partial t}(\rho_s(1-\phi))+\nabla\cdot(\rho_s(1-\phi)\mathbf{v}_s)=-\Gamma_l. \tag{2}$$

Neglecting kinetic energy, the rate at which surface stresses do work on the solid and liquid, the work done by body forces, and assuming there is no internal heat production, and given that the mixed phase region is assumed to be in local thermodynamic equilibrium, the statement of conservation of energy in the mixed phase region may be expressed as [1, 19]

$$\nabla\cdot(\mathbf{k}_m\nabla\cdot T)=L\Gamma_l+[(1-\phi)\rho_s c_p^s+\phi\rho_l c_p^l]\frac{\partial T}{\partial t}+(1-\phi)\rho_s c_p^s\mathbf{v}_s\cdot\nabla T+\phi\rho_l c_p^l\mathbf{v}_l\cdot\nabla T \tag{3}$$

with

$$\mathbf{k}_m=(1-\phi)\mathbf{k}_s+\phi\mathbf{k}_l. \tag{4}$$

Derivation of the statement of conservation of linear momentum in the mixed phase region requires specific consideration of its structure and rheology. Assuming that the pressures in the solid and liquid phases are equal, that both phases may be treated as Newtonian fluids which are incompressible at the microscale, that the rate of change of momentum in each can be neglected, that the Reynolds number of each is small compared to unity, and that the body force acting upon each phase is due only to gravity, then conservation of linear momentum in the liquid and solid may be expressed as [1]

$$\nabla\cdot(\phi\boldsymbol{\sigma}_l)-\rho_l\phi g\hat{k}-\mathbf{I}=0 \tag{5}$$

$$\nabla\cdot((1-\phi)\boldsymbol{\sigma}_s)-\rho_s(1-\phi)g\hat{k}+\mathbf{I}=0. \tag{6}$$

Note that the interphase force per unit volume ($\mathbf{I}$) acting upon the solid is equal and opposite to that acting upon the liquid, and so satisfies Newton's third law [26]. The interphase force per unit volume may be expressed as

$$\mathbf{I}=\mathbf{C}(\mathbf{v}_l-\mathbf{v}_s)-P\nabla\phi \tag{7}$$

where the value of $\mathbf{C}$ depends upon the distribution of phases within the mixed phase region [19]. Substituting equation (7), and the standard equation for the stress tensor within an incompressible fluid [27] into equation (5), and simplifying, yields

$$\mathbf{v}_l-\mathbf{v}_s=-\frac{\phi}{\mathbf{C}}\nabla(P+\rho_l gz). \tag{8}$$

If $\mathbf{v}_s=0$ then equation (8) corresponds to D'Arcy's law with

$$\mathbf{C}=\mu_l\phi^2/k. \tag{9}$$

The deformable solid matrix will expel the liquid phase if subjected to isostatic compression, and may be treated on the macroscopic scale as a viscous, compressible fluid [19, 28]. Substituting equations (7), (9), and the standard equation for the stress tensor within a compressible fluid [27] into equation (6), and simplifying assuming that the bulk and shear viscosities of the matrix are constant, yields

$$\nabla(P+\rho_l gz)=(\xi_s+\tfrac{1}{3}\mu_s)\nabla(\nabla\cdot\mathbf{v}_s)+\mu_s\nabla^2\mathbf{v}_s-(1-\phi)(\rho_s-\rho_l)g\hat{k}. \tag{10}$$

Summation of equations (8) and (10), having substituted for $\mathbf{C}$ in equation (8) using equation (9), yields the statement of conservation of linear momentum in the mixed phase region, valid if the liquid volume fraction does not exceed the CMF [19]

$$\left(\xi_s+\frac{1}{3}\mu_s\right)\nabla(\nabla\cdot\mathbf{v}_s)=\frac{\mu_l\phi}{k}(\mathbf{v}_l-\mathbf{v}_s)-\mu_s\nabla^2\mathbf{v}_s+(1-\phi)(\rho_s-\rho_l)g\hat{k}. \tag{11}$$

Practical use of this expression requires that the permeability of the solid matrix be specified. Generally, for an isotropic matrix, permeability may be related to porosity by an equation of the form

$$k=ba^2f(\phi) \tag{12}$$

where b is a constant, and a is the radius of the solid grains [29]. The form of $f(\phi)$ and value of b depend upon the microscopic distribution of the liquid phase. Several expressions for $f(\phi)$ have been proposed [e.g. 28, 29]; a simple, commonly used form, based on the Blake–Kozeny–Carman equation, yields the permeability–porosity expression

$$k=ba^2\phi^n \tag{13}$$

where n varies between 2 and 3 [28].

2.2. *Phase compositions and the rate of phase change*

To close the system of conservation equations, the rate of phase change and the composition of each phase must be specified. The rate of phase change is dictated by the rate at which the phases experience changing thermodynamic conditions; in this system, a phase may experience changing thermodynamic conditions both because the conditions throughout the mixed phase region are changing temporally, and because the phases are migrating through conditions which vary spatially. Migration may occur because the mixture itself is mobile, and because the phases migrate relative to the mixture. Consequently, the net

rate of change of thermodynamic conditions experienced by the phases at any point is given by

$$\dot{f}(P,T) = \frac{\partial}{\partial t}(f(P,T)) + (\mathbf{v}_l + \mathbf{v}_s - \mathbf{v}_m)\cdot\nabla(f(P,T)) \tag{14}$$

where $\mathbf{v}_m$ is the mass averaged mixture velocity

$$\mathbf{v}_m = \rho_l\phi\mathbf{v}_l/\rho_m + \rho_s(1-\phi)\mathbf{v}_s/\rho_m \tag{15}$$

and the mixture density is given by

$$\rho_m = \phi\rho_l + (1-\phi)\rho_s. \tag{16}$$

If a system is in local thermodynamic equilibrium, phase change may be related to the thermodynamic conditions by a suitable equilibrium phase diagram or phase distribution curve [1, 3, 4, 9]. Phase distribution curves give the volume fraction and composition of each phase present at given thermodynamic conditions; they have been derived for several commonly occurring silicate rock types [e.g. 30–32]. Once the equilibrium liquid volume fraction v_l is known as a function of the thermodynamic conditions, equation (14) may be rewritten in terms of $\rho_l v_l$, and the rate of solid–liquid phase change is given by

$$\Gamma_l = \dot{f}(P,T) = \frac{\partial\rho_l v_l}{\partial t} + (\mathbf{v}_l + \mathbf{v}_s - \mathbf{v}_m)\cdot\nabla(\rho_l v_l). \tag{17}$$

The second term on the right-hand side of equation (17) demonstrates that relative phase transport coupled with local thermodynamic equilibration leads to component exchange between solid and liquid phases. A full continuum description of a multicomponent system would strictly require an explicit statement of conservation of mass for each component, but for most geological materials this would lead to a prohibitive increase in the complexity of the formulation due to the large number of components present [9]. In the system discussed here, phase compositions are fixed by the requirement of local thermodynamic equilibrium, and may be deduced at given thermodynamic conditions using empirical data derived from equilibrium melting experiments. Consequently, we neglect an explicit description of mass conservation for each component. We believe this approach is no less rigorous than one in which macroscopic continuum equations for each component are explicitly stated, because in the absence of an atomic level description of the system, component exchange must in any case be deduced from empirical data [1, 3, 4].

2.3. *A one-dimensional Boussinesq model of the mixed phase region*

Equations (1), (2), (3), (11), (13) and (17) together with the necessary empirical data represent a complete description of the system, but the task of solving them would be considerable. At this stage, in order to identify the generic features of the system, we will consider a simplified one-dimensional (1-D) subset of the governing equations and investigate the solutions numerically. An understanding of the essential physics may then lead to the solution of more complex formulations.

Expressed only in terms of vertical velocity components, the governing equations become

$$\frac{\partial}{\partial t}(\rho_l\phi) + \frac{\partial}{\partial z}(\rho_l\phi w_l) = \Gamma_l \tag{18}$$

$$\frac{\partial}{\partial t}(\rho_s(1-\phi)) + \frac{\partial}{\partial z}(\rho_s(1-\phi)w_s) = -\Gamma_l \tag{19}$$

$$\frac{\partial}{\partial z}\left(\mathbf{k}_m\frac{\partial T}{\partial z}\right) = L\Gamma_l + [(1-\phi)\rho_s c_p^s + \phi\rho_l c_p^l]\frac{\partial T}{\partial t} + (1-\phi)\rho_s c_p^s w_s\frac{\partial T}{\partial z} + \phi\rho_l c_p^l w_l\frac{\partial T}{\partial z} \tag{20}$$

$$\left(\xi_s + \frac{4}{3}\mu_s\right)\frac{\partial^2 w_s}{\partial z^2} = \frac{\mu_l\phi}{k}(w_l - w_s) + (1-\phi)(\rho_s - \rho_l)g \tag{21}$$

$$\Gamma_l = \frac{\partial\rho_l v_l}{\partial t} + (w_l + w_s - w_m)\frac{\partial\rho_l v_l}{\partial z} \tag{22}$$

subject to the initial and boundary conditions

$$T(z,0) = T_{sol} \tag{23a}$$

$$\phi(z,0) = v_l(z,0) = w_l(z,0) = w_s(z,0) = 0 \tag{23b}$$

$$T(0,t) = T_b \quad T(z_{sol},t) = T_{sol} \tag{23c}$$

$$v_l(0,t) = v_b^l \quad v_l(z_{sol},t) = 0 \tag{23d}$$

$$w_l(0,t) = w_s(0,t) = w_l(z_{sol},t) = w_s(z_{sol},t) = 0 \tag{23e}$$

where v_b^l denotes the equilibrium liquid volume fraction at $z = 0$, and z_{sol} denotes the time-dependent position of the solidus isotherm, which defines the "top" of the mixed phase region (Fig. 1).

Applying the Boussinesq approximation, substituting equation (18) in equation (19), and integrating subject to the condition that $w_s = w_l = 0$ at $z = 0$ yields [19]

$$\phi w_l = -(1-\phi)w_s. \tag{24}$$

Assuming that the thermodynamic properties of the solid and liquid are constant and identical, substituting equation (24) into equations (18)–(22), and simplifying yields

$$\rho\frac{\partial\phi}{\partial t} - \rho\frac{\partial}{\partial z}((1-\phi)w_s) = \Gamma_l \tag{25}$$

$$\mathbf{k}\frac{\partial^2 T}{\partial z^2} = \rho c_p\frac{\partial T}{\partial t} + L\Gamma_l \tag{26}$$

$$\left(\xi_s + \frac{4}{3}\mu_s\right)\frac{\partial^2 w_s}{\partial z^2} = (1-\phi)(\rho_s - \rho_l)g - \frac{\mu_l w_s}{k} \tag{27}$$

$$\Gamma_l = \rho \frac{\partial v_l}{\partial t} + \rho(w_l + w_s)\frac{\partial v_l}{\partial z}. \quad (28)$$

Note that in the heat conservation equation (26), the velocity terms which describe advective heat transport have now cancelled. Physically, this is because the upwards advection of hot liquid is exactly balanced by the downwards advection of cold solid, so heat transport occurs only by conduction and latent heat exchange during phase change.

Phase change due to heating may be expressed as a function of temperature only, and for simplicity a linear variation of equilibrium liquid volume fraction with temperature will be used

$$v_l = \frac{T - T_{sol}}{T_{liq} - T_{sol}}. \quad (29)$$

This is a reasonable approximation for a range of silicate rock types [30–32]. In addition, latent heat will be assumed to be released linearly as phase change proceeds [33]. A convenient scheme for non-dimensionalizing temperature may be obtained from equation (29); by writing

$$T' = \frac{T - T_{sol}}{T_{liq} - T_{sol}} \quad (30)$$

the dimensionless temperature T' is numerically equivalent to the equilibrium liquid volume fraction v_l. In the interests of clarity, a new variable θ will be invoked which represents both these quantities; i.e. $\theta = T' = v_l$. Liquid volume fractions may be normalized by writing

$$\theta' = \theta/\varphi, \quad (31a)$$

$$\text{with} \quad \varphi = \frac{T_b - T_{sol}}{T_{liq} - T_{sol}}$$

$$\phi' = \phi/\varphi, \quad (31b)$$

where the scaling factor φ denotes both the equilibrium liquid volume fraction, and the dimensionless temperature, at $z = 0$; i.e. $\varphi = T'_b = v^l_b$. Assuming a constant density contrast and liquid shear viscosity, the remaining variables may be non-dimensionalized by writing [19]

$$z' = z/\delta, \quad \text{with } \delta = \left(\frac{(\xi_s + 4\mu_s/3)K}{\mu_l}\right)^{1/2} \quad (32)$$

$$t' = t/\tau, \quad \text{with } \tau = \frac{1}{(1-\varphi)(\rho_s - \rho_l)g}\left(\frac{\mu_l(\xi_s + 4\mu_s/3)}{K}\right)^{1/2} \quad (33)$$

$$w' = w/\omega, \quad \text{with } \omega = \frac{K(1-\varphi)(\rho_s - \rho_l)g}{\mu_l} \quad (34)$$

$$k' = k/K, \quad \text{with } K = ba^2\varphi^n. \quad (35)$$

Substituting equation (28) into equations (25) and (26), substituting equation (13) into equation (27), substituting the scaled and dimensionless variables (31)–(35), simplifying, and dropping primes yields the dimensionless governing equations

$$\frac{\partial \phi}{\partial t} = \frac{1}{\varphi}\frac{\partial}{\partial z}((1-\varphi\phi)w_s) + \frac{\partial \theta}{\partial t} + (w_l + w_s)\frac{\partial \theta}{\partial z} \quad (36)$$

$$\frac{\partial \theta}{\partial t} = \kappa_{eff}\frac{\partial^2 \theta}{\partial z^2} - Ste(w_l + w_s)\frac{\partial \theta}{\partial z} \quad (37)$$

$$\frac{\partial^2 w_s}{\partial z^2} = \frac{w_s}{\phi^n} + \frac{(1-\varphi\phi)}{(1-\varphi)} \quad (38)$$

$$\varphi\phi w_l = -(1-\varphi\phi)w_s \quad (39)$$

with

$$\kappa_{eff} = \frac{k\tau}{\rho c_{eff}\delta^2} \quad (40)$$

$$Ste = \frac{L}{c_{eff}(T_{liq} - T_{sol})} \quad (41)$$

$$c_{eff} = c_p + \frac{L}{T_{liq} - T_{sol}}. \quad (42)$$

We have chosen not to substitute for w_l using equation (39), because in this form, the effect of the net phase velocity $(w_l + w_s)$ on the governing equations is clear. The initial and boundary conditions become

$$\theta(z,0) = \phi(z,0) = w_s(z,0) = w_l(z,0) = 0 \quad (43a)$$

$$\theta(0,t) = 1 \quad \theta(z_0,t) = 0 \quad (43b)$$

$$w_s(0,t) = w_l(0,t) = w_s(z_0,t) = w_l(z_0,t) = 0 \quad (43c)$$

where z_0 denotes the position of the $\theta = 0$ isotherm.

As discussed by [9, 15], the results of binary and multicomponent phase change models are difficult to generalize, because of the large number of governing parameters and wide variety of naturally occurring equilibrium phase fraction distributions. Using suitable approximations, assuming a linear equilibrium liquid volume fraction distribution, and non-dimensionalizing, we have reduced the model description to a system of four coupled equations in four unknowns, governed by four externally prescribed dimensionless parameters: κ_{eff}, Ste, n and φ. The equations are amenable to solution using standard numerical techniques; in the next section we present the results of numerical experiments designed to characterize the system in terms of the external parameters.

3. RESULTS

Equations (36)–(39) were approximated using explicit finite difference schemes [34], and solved numerically using FORTRAN codes [35] processed on a Sun SPARC 5 workstation. CPU times increased with increasing κ_{eff}, from several minutes to several hours. Accuracy of the finite difference scheme for equation (37) was tested against a published analytic approximation to the solution of a diffusion–advection problem [36]; accuracy of the scheme for equa-

tions (36) and (38) was tested against the published analytic solution for a solitary porosity wave with $n = 3$, no phase change ($\Gamma_1 = 0$), and in the limit of small background porosity [21]. All numerical experiments were performed using a value of $n = 3$, to allow comparison with the analytic solution.

We chose to investigate the numerical solutions for a variety of values of φ and *Ste*, over a fixed range of κ_{eff} between $\sim 10^{-8}$ and $\sim 10^{+8}$. This range is representative of most silicate rock phase change systems, and its size reflects the uncertainty in estimated values of the matrix bulk and shear viscosities, which appear in the definition of κ_{eff} [equation (40)]. The resistance of the matrix to deformation by liquid enhanced creep processes is governed by the diffusion of components along grain boundaries [17]. The bulk and shear viscosities are, therefore, functions of the diffusion rates of individual components, and of the porosity and grain size, which dictate the effective diffusion lengthscale [17, 18]. Diffusion rates are poorly constrained, and their effect upon the bulk and shear viscosities of a deformable, *multicomponent* mush is unknown. Consequently, matrix bulk and shear viscosities are poorly constrained; estimates for partially molten rocks range from 10^{15} to 10^{21} Pa s.

Neither φ or *Ste* are independent of κ_{eff}; substituting equations (32) and (33) into equation (40) reveals that κ_{eff} varies with φ as

$$\kappa_{\text{eff}} \sim 1/(1-\varphi)\varphi^{9/2} \tag{44}$$

while both *Ste* and κ_{eff} are governed by the values of the thermal parameters L, c_p, T_{liq} and T_{sol}. However, re-writing the expression for the Stefan number as

$$Ste = \frac{L}{c_p(T_{\text{liq}} - T_{\text{sol}}) + L} \tag{45}$$

it is clear that it is constrained to lie between 0 and 1, whereas for a fixed value of *Ste*, κ_{eff} may still vary over effectively our entire chosen range. Consequently, in all our numerical experiments we have assumed *Ste* is independent of κ_{eff}.

3.1. *Relative importance of conduction and pseudo-advection during heat transport*

Models of heat transport within a mush often assume conduction is the dominant transport mechanism, implicitly assuming that phase transport has negligible effect on heat transport [6, 7, 9]. In our model, phase transport affects heat transport due to the exchange of latent heat during local thermal equilibration, and is described in the energy conservation equation (37) by the second term on the right-hand side, which we refer to as a 'pseudo-advection' term. Heat transport is governed externally by the dimensionless effective thermal diffusivity (κ_{eff}), and the Stefan number (*Ste*). The Stefan number represents the ratio of latent heat to effective specific heat during phase change; for $Ste = 1$ all heat is exchanged as latent heat, while for $Ste = 0$ all heat is absorbed as specific heat.

To assess the importance of phase transport on heat transport, the governing equations were solved with $Ste = 1$ (maximum pseudo-advection), and with $Ste = 0$ (conduction only). The difference between the resulting thermal profiles was measured as a function of κ_{eff} by recording the difference between the positions of selected isotherms, and normalizing them to the conductive case

$$D_i = \frac{z_{i(Ste=1)} - z_{i(Ste=0)}}{z_{i(Ste=0)}}. \tag{46}$$

A value of $D_i = 0$ indicates that the isotherm positions are identical, and that heat transport is dominated by conduction, whilst a value of $D_i = 1$ indicates that they differ significantly and that heat transport is dominated by pseudo-advection. Figure 2 shows the normalized difference between the $z_{0.6}$, $z_{0.2}$ and z_0 isotherms after 30 time units, as a function of κ_{eff}, for three values of φ. In all cases, for large values of κ_{eff} heat transport is dominated by conduction. With decreasing κ_{eff}, pseudo-advection becomes increasingly important, and dominates for values of κ_{eff} in the range 10^{-7}–10^{-2}. Conduction then becomes increasingly significant for small as well as large values of κ_{eff}.

Lowell and Bergantz [25] investigated heat transport in a deformable binary mushy zone heated from below, and concluded that for large κ_{eff} (their "dimensionless conduction lengthscale") and small *Ste*, heat transport is dominated by conduction, whilst for small κ_{eff} and large *Ste*, heat transport is dominated by pseudo-advection (their "compaction dominated"). Their treatment neglects the effect of the net phase velocity ($w_l + w_s$) on the magnitude of the pseudo-advection term, and consequently fails to predict the increasing significance of conduction for *small* values of κ_{eff}, which, as discussed in Section 3.2, is due to the effect of the net phase velocity.

3.2. *Form of the liquid volume fraction (porosity) distributions*

Figure 3(a)–(d) shows a representative selection of normalized spatial porosity and equilibrium liquid volume fraction (dimensionless temperature) distributions, for the case $\varphi = 0.5$, after 30 time units have elapsed. For large κ_{eff} ($\geqslant 10^5$), there is little difference between the porosity and the equilibrium liquid fraction distributions [Fig. 3(a)]. For κ_{eff} between $\sim 10^4$ and ~ 10, the upwardly migrating liquid develops a high amplitude "porosity wave", and trailing porosity waves begin to develop behind the leading wave [Fig. 3(b)]. In this range, as κ_{eff} decreases, the amplitude of the leading wave increases, and the position of the porosity maximum moves closer to z_0. For κ_{eff} between ~ 10 and $\sim 10^{-3}$, the trailing waves are well developed, and display decreasing amplitude with depth [Fig. 3(c)]. In this range,

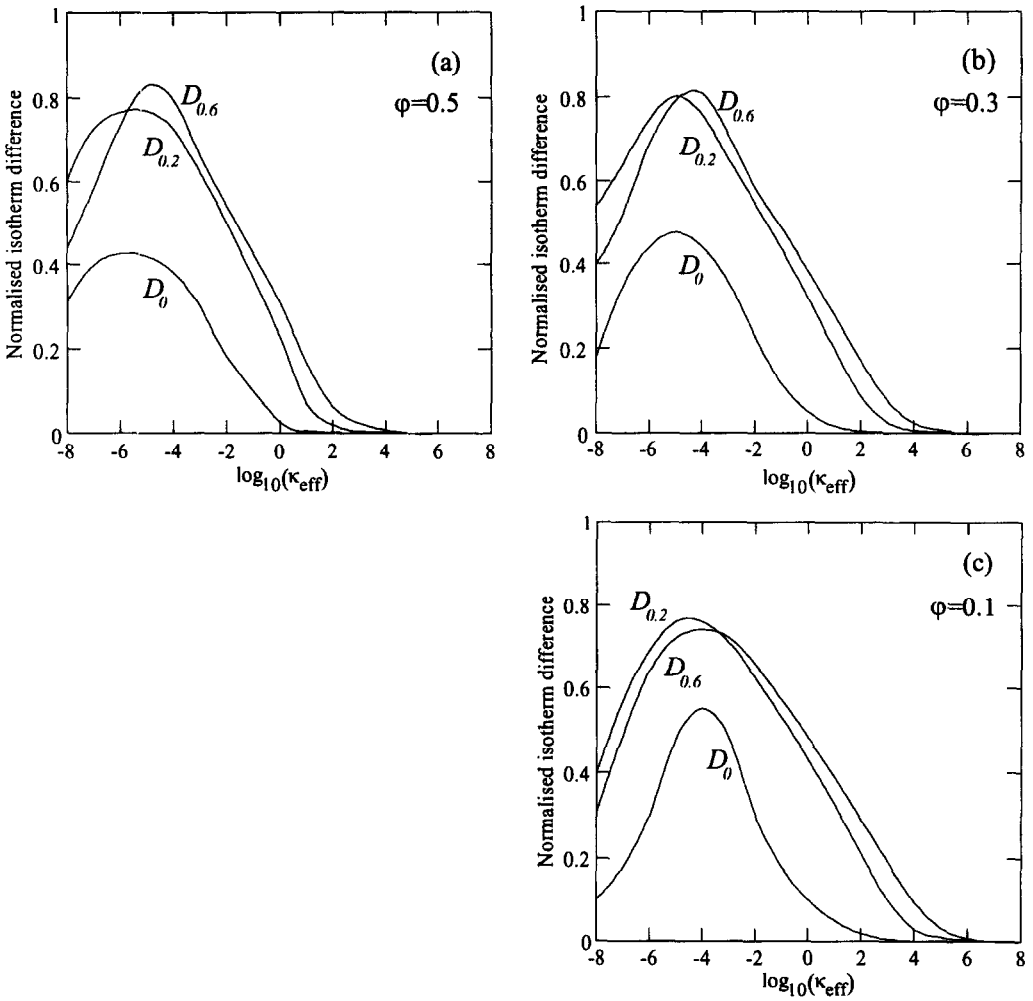

Fig. 2. Normalized difference between the $z_{0.6}$, $z_{0.2}$ and z_0 isotherms for the $Ste = 1$ (maximum pseudo-advection) and $Ste = 0$ (conduction only) cases, as a function of κ_{eff}, after 30 time units, with: (a) $\varphi = 0.5$; (b) $\varphi = 0.3$; (c) $\varphi = 0.1$.

as κ_{eff} decreases, the amplitude of the leading wave decreases, the position of the porosity maximum moves closer to z_0, and the wave frequency increases. For small κ_{eff} ($\leqslant 10^{-4}$), the porosity distribution breaks down into a series of upwardly propagating, small amplitude waves [Fig. 3(d)].

The spatial porosity distribution depends upon the relative rates of upward transport of liquid and heat, which for a particular value of φ is primarily governed by the magnitude of κ_{eff}. Using equations (37) and (39), the mass conservation equation (36) may be written in a form more open to physical interpretation

$$\frac{\partial \phi}{\partial t} = -C + \kappa_{eff}\frac{\partial^2 \theta}{\partial z^2} + (1 - Ste)(w_l + w_s)\frac{\partial \theta}{\partial z} \quad (47)$$

with

$$C = \frac{\partial}{\partial z}(\phi w_l). \quad (48)$$

The first term on the right-hand side of equation (47), C, governs the compaction rate, and demonstrates that gradients in the liquid phase flux (ϕw_l) cause local changes in porosity. If the liquid phase flux at any point increases with height the compaction rate (C) is positive, the porosity locally decreases, and the deformable matrix *compacts* to occupy the space previously occupied by liquid. Conversely, if the liquid phase flux decreases with height the compaction rate is negative, the porosity locally increases, and the deformable matrix *dilates* to accommodate the accumulating liquid. The second and third terms are source terms which describe phase change due to conductive heat transport, and phase change due to pseudo-advective heat transport respectively.

For the case $Ste = 1$, the pseudo-advective source term is zero, so porosity change is governed by the relative magnitudes of the compaction and conduction terms only. Large values of κ_{eff} result from conditions which promote slow liquid transport but rapid conductive heat transport, such as small matrix grain size, high liquid phase viscosity, and high ther-

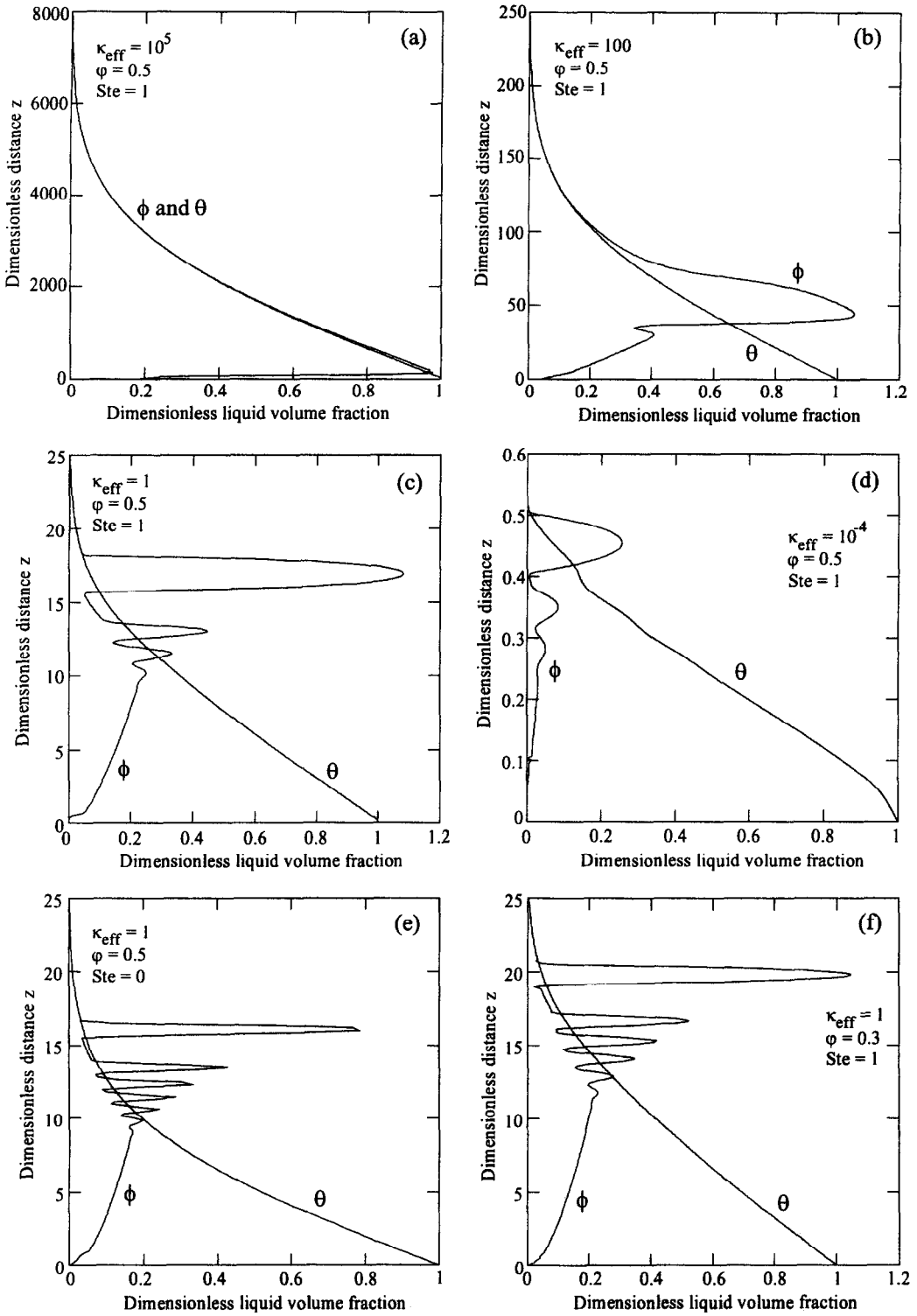

Fig. 3. Normalized spatial porosity and equilibrium liquid volume fraction distributions, after 30 time units, with: (a) $\kappa_{eff} = 10^5$, $\varphi = 0.5$, $Ste = 1$; (b) $\kappa_{eff} = 100$, $\varphi = 0.5$, $Ste = 1$; (c) $\kappa_{eff} = 1$, $\varphi = 0.5$, $Ste = 1$; (d) $\kappa_{eff} = 10^{-4}$, $\varphi = 0.5$, $Ste = 1$; (e) $\kappa_{eff} = 1$, $\varphi = 0.5$, $Ste = 0$; (f) $\kappa_{eff} = 1$, $\varphi = 0.3$, $Ste = 1$. Liquid volume fractions are normalized to the equilibrium liquid volume fraction at $z = 0$ (φ). Note both ordinate and abscissa axis scales differ between plots.

mal conductivity [equation (40)]. Consequently, for large κ_{eff}, the conductive heat transport term dominates the compaction term, and equation (47) can be approximated as

$$\frac{\partial \phi}{\partial t} \approx \frac{\partial \theta}{\partial t} \approx \kappa_{\text{eff}} \frac{\partial^2 \theta}{\partial z^2}. \tag{49}$$

As κ_{eff} decreases, the rate of liquid phase transport increases relative to the rate of heat transport, until the liquid phase migrates upwards faster than the dimensionless solidus isotherm, z_0. At z_0 the porosity and hence permeability falls to zero, so upward migrating liquid must accumulate below it, resulting in the development of a porosity wave. In the region immediately below a porosity wave, the liquid phase flux increases with height, the compaction term is positive, so the porosity locally decreases. If the relative rate of liquid transport is sufficiently high that the compaction term in equation (47) dominates the conduction term, then trailing porosity waves develop, because compaction leads to a reduction in the permeability for which the creation of liquid by phase change cannot compensate. This acts as a local restriction to liquid transport, below which liquid accumulates and a new porosity wave develops. As the relative rate of liquid transport increases, so the local compaction rate below an incipient porosity wave increasingly outstrips the rate of phase change, leading to an increase in the wave frequency.

When κ_{eff} becomes very small, the conductive heat transport term in equation (47) becomes very small. Consequently, too little liquid is produced by phase change for a large amplitude porosity wave to develop. The generally low permeabilities inhibit phase transport, so phase velocities are low, the net phase velocity is small, and the pseudo-advective term in the energy conservation equation (37) is also small. Consequently, heat transport is dominated by conduction for small values of κ_{eff}, as observed in Fig. 2.

For the case $Ste = 0$, the pseudo-advective source term in equation (47) exerts maximum influence on the porosity distribution. Figure 3(e) illustrates the effect of this, and should be compared with Fig. 3(c); the most significant differences are that the amplitude of the leading porosity wave is reduced, and the wave frequency increased. Because $\partial\theta/\partial z$ is always negative, if $|w_l| > |w_s|$, the pseudo-advection term in equation (47) is negative, and so acts to reduce the porosity. Physically, this is because the rate at which liquid is migrating upwards (w_l) into cooler regions and freezing is greater than the rate at which solid is migrating downwards (w_s) into hotter regions and melting. Consequently, less liquid is produced by phase change, and porosity waves are more efficiently generated by compaction.

The effect of reducing φ is illustrated by Fig. 3(f), which again should be compared with Fig. 3(c). The amplitude of the leading porosity wave is similar in both cases, but the wave frequency is increased. This is because, over the range $0 < \varphi < 0.8$, κ_{eff} effectively varies with φ as

$$\kappa_{\text{eff}} \sim 1/\varphi^{9/2}. \tag{50}$$

Consequently, reducing φ at constant κ_{eff} is *qualitatively* similar to reducing κ_{eff} at constant φ, because reducing φ causes the range of values of κ_{eff} available from varying the other constituent variables to be shifted upwards. The changes are *quantitatively* different because φ also appears independently in the momentum conservation equation (38).

Figure 4(a) shows dimensionless liquid and matrix velocities for the case $\kappa_{\text{eff}} = 1$, $Ste = 1$, and $\varphi = 0.5$, after 30 time units, and should be compared with Fig. 3(c). Positive liquid velocities reflect the upwards migration of buoyant liquid; negative solid velocities reflect the downwards migration of matrix. Changes in velocity correlate with changes in porosity, because the permeability is governed by the local porosity. Figure 4(b) shows the dimensionless compaction rate (C) and matrix strain rate ($\partial w_s/\partial z$), for the same parameters, and should again be compared with Fig. 3(c). Negative compaction rates above local porosity maxima demonstrate that the porosity is increasing; conversely, positive compaction rates below local porosity maxima demonstrate that the porosity is decreasing. The association of negative and positive compaction rates with each porosity wave causes new waves to develop below existing waves, and existing waves to migrate upwards. The effect of this on the matrix is demonstrated by the matrix strain rate; negative compaction rates correlate with positive (dilating) strain rates, and vice-versa.

3.3. *Increase in maximum porosity with time: formation of a slurry*

If the amplitude of the porosity waves continually increases with time, then the local volume fraction may eventually exceed the CMF, in which case the contiguity of the solid matrix grains will break down, and the rheological description of that part of the mixed phase region will change from mush to slurry [4, 9]. The mush-slurry transition is important, because the liquid fraction of the slurry has effectively segregated from the mush. A slurry is mobile, and if a suitable route is made available, may migrate away from the mushy zone.

Figure 5 shows a representative selection of the maximum normalized porosity against time curves. For large κ_{eff} ($\geqslant 10^5$), the maximum porosity changes little with time [Fig. 5(a)]. For κ_{eff} between $\sim 10^4$ and $\sim 10^{-3}$, the rate of increase of maximum porosity is rapid with time [Fig. 5(b) and (c)]; for small values of κ_{eff} ($\leqslant 10^{-4}$), the maximum porosity initially falls until the slope abruptly changes and the maximum porosity begins to increase, although the rate of increase is slow [Fig. 5(d)]. Because the momentum conservation equation (38) is valid only if $\varphi <$ CMF, the mush-slurry transition is possible only in systems

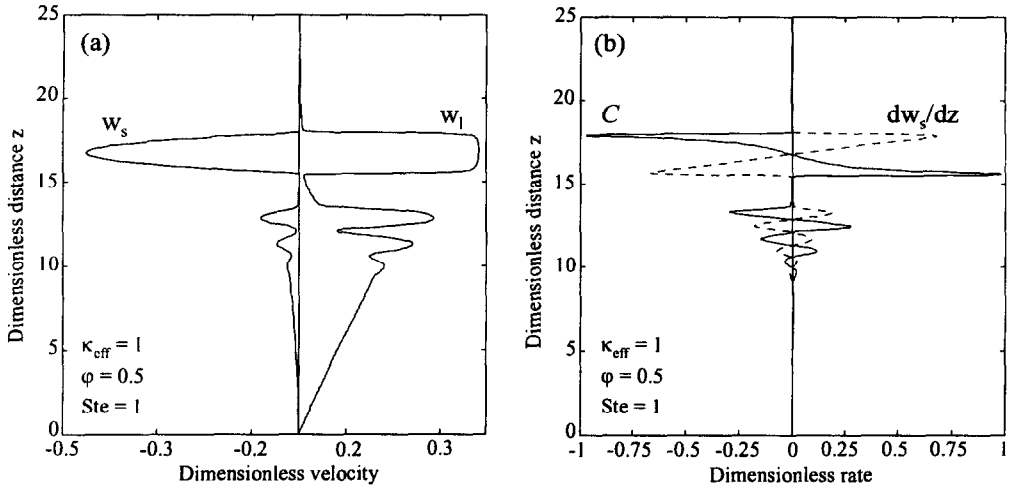

Fig. 4. Results for the case $\kappa_{eff} = 1$, $\varphi = 0.5$, $Ste = 1$, after 30 time units: (a) dimensionless liquid and solid velocities; (b) dimensionless compaction rate (C) and matrix strain rate.

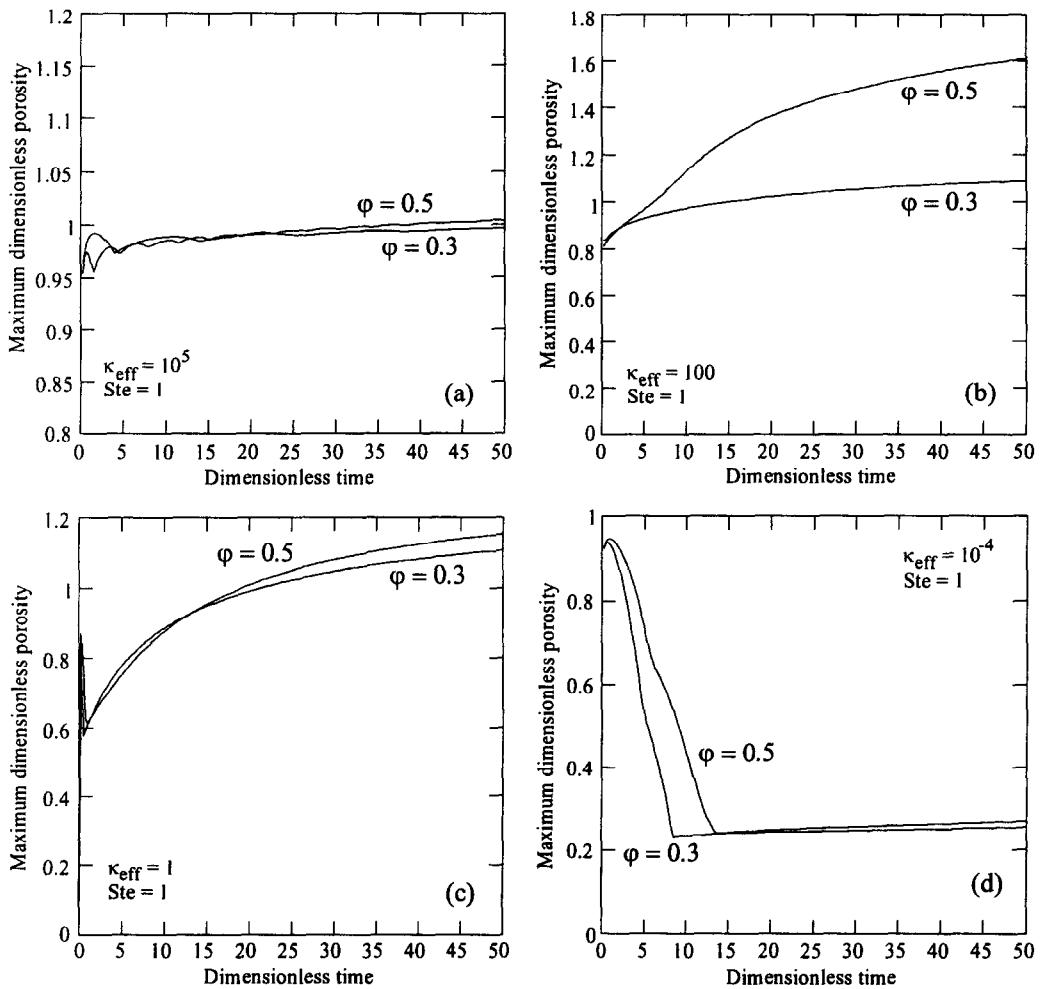

Fig. 5. Maximum normalized porosity as a function of dimensionless time, for the $\varphi = 0.5$ and 0.3 cases, with: (a) $\kappa_{eff} = 10^5$; (b) $\kappa_{eff} = 100$; (c) $\kappa_{eff} = 1$; (d) $\kappa_{eff} = 10^{-4}$. In all cases, $Ste = 1$. Porosity is normalized to the equilibrium liquid volume fraction at $z = 0$ (φ). Note abscissa scale differs between plots.

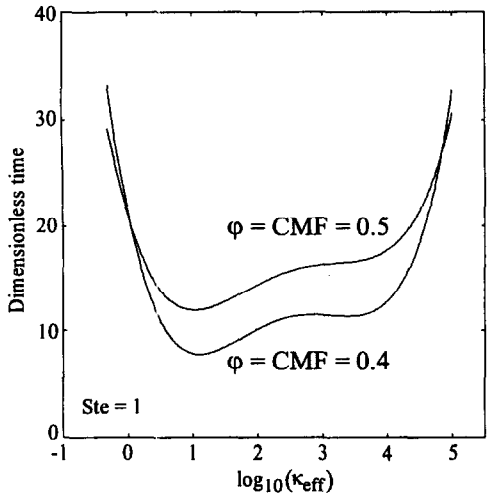

Fig. 6. Segregation time as a function of κ_{eff}, for φ = CMF = 0.5, and φ = CMF = 0.3. *Ste* = 1.

in which the maximum normalized porosity eventually exceeds 1; the results obtained indicate that slurry formation is possible for κ_{eff} in the range $\sim 10^{5}$–$\sim 10^{-3}$.

The model may be used to estimate the time required to *initiate* the mush-slurry transition, which we term the segregation time, by recording the time required for the porosity at any point to reach the CMF. For a system in local mechanical and thermodynamic equilibrium, the CMF lies in the range 0.4–0.6 [14]. Figure 6 shows an example of the segregation time as a function of κ_{eff}, for *Ste* = 1, with φ = CMF = 0.5 and φ = CMF = 0.3. These are convenient approximations to the situation in which the equilibrium liquid fraction at $z = 0$ (φ) lies fractionally below the CMF, and represent the shortest segregation times for the chosen parameters. Segregation times are shortest in the range $1 < \kappa_{eff} < 10^{4}$; the segregation time then increases with both decreasing and increasing κ_{eff}. A maximum dimensionless time of 100 was imposed, to avoid excessive computational expense.

3.4. *Compositional consequences of local thermodynamic equilibrium*

Figure 7(a) shows a plot of the normalized dimensionless temperature at the point of incipient mush–slurry transition as a function of κ_{eff}, for the system described in Section 3.3. For small κ_{eff}, the mush–slurry transition occurs in the coolest part of the mixed phase region just below the solidus isotherm. As κ_{eff} increases, the mush–slurry transition occurs in hotter parts of the mixed phase region, because the position of the porosity maximum lags further behind z_0. The temperature at the point of incipient mush–slurry transition depends upon the values of φ, κ_{eff} and the value of the CMF.

The requirement of local thermodynamic equilibrium allows the composition of the incipient slurry to be deduced by combining Fig. 7(a) with empirical phase change data. Figure 7(b) shows an example of the equilibrium liquid phase composition in terms of oxides, for a common lower crustal rock. For a system with $\kappa_{eff} \approx 3$, the dimensionless temperature at the point of slurry formation is $\theta \approx 0.2$ [Fig. 7(a)]; the composition of the liquid fraction of the slurry at a dimensionless temperature of $\theta \approx 0.2$ would be described as granitic [Fig. 7(b)]. In like fashion, it may be deduced that, with increasing κ_{eff}, the composition of the liquid part of the slurry would evolve to tonalitic through to granodioritic. The significant result is that, because the liquid phase in the porosity wave has thermodynamically equilibrated at low temperatures near the top of the mixed phase region, the composition of the liquid fraction of the mobile slurry corresponds to only a small fraction (<0.05–0.4) of equilibrium melting of the starting material, despite the liquid fraction in the slurry having accumulated until it exceeded the CMF.

4. CONCLUSIONS

The transport of heat, mass and momentum in a deformable much undergoing solid–liquid phase change has, for a simple 1-D system heated from below, been characterized in terms of four externally prescribed dimensionless parameters: the effective thermal diffusivity, κ_{eff}; the Stefan number, *Ste*; the equilibrium liquid fraction at $z = 0$, φ (which is numerically equivalent to the dimensionless temperature at $z = 0$); and the exponent in the permeability relation, n.

Heat transport is governed externally by κ_{eff} and *Ste*, and depends also upon the net phase velocity $(w_l + w_s)$. For large values of *Ste*, heat transport is dominated by phase transport over a wide range of values of κ_{eff}. Caution must therefore be exercised when describing the heat transport in a deformable mushy zone; for many systems a conductive only formulation will be inadequate. The spatial distribution of the liquid volume fraction (porosity) depends upon the relative transport rates of heat and liquid, and for a specific value of φ is effectively governed by the magnitude of κ_{eff}. For a wide range of values of κ_{eff}, the liquid fraction accumulates below the solidus isotherm, and a porosity wave develops. The amplitude of this wave increases with time, until the contiguity of the solid matrix breaks down, and the rheological description of that part of the mixed phase region changes from mush to slurry. The composition of the slurry depends upon both the initial composition of the material, and the values of κ_{eff}, φ, and the CMF. For $\kappa_{eff} \leqslant 10^{2}$, the composition of the liquid fraction of the slurry corresponds to only a small fraction of equilibrium melting of the material, because incipient slurry formation occurs near the top of the mixed phase region where temperatures are low.

This paper was originally motivated by the need to understand coupled phase change and phase transport

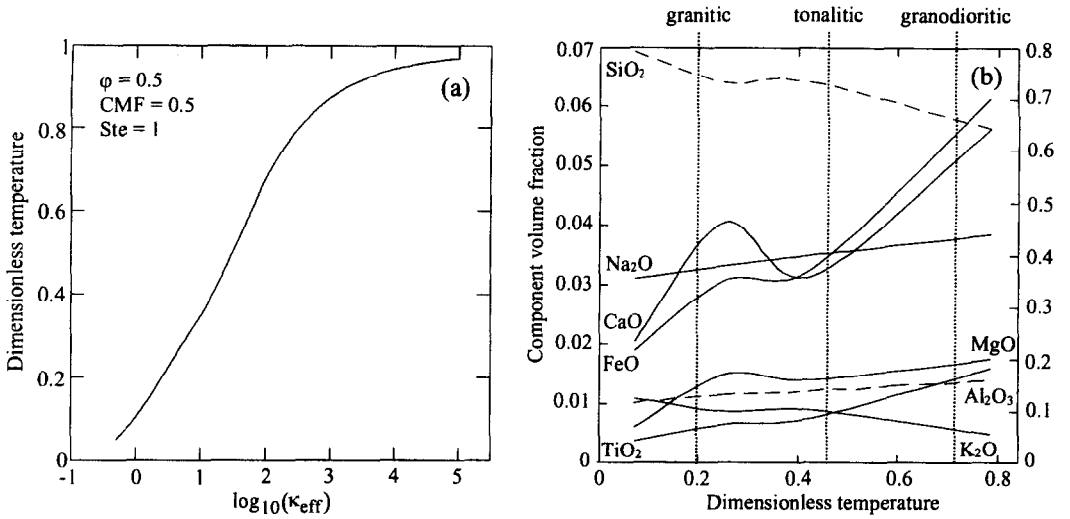

Fig. 7. (a) Normalized dimensionless temperature at the position of incipient slurry formation, as a function of κ_{eff}. $\varphi = 0.5$; CMF = 0.5; $Ste = 1$. Dimensionless temperature is normalized to the dimensionless temperature at $z = 0$ (φ). (b) Component oxide volume fractions as a function of normalized dimensionless temperature, for an andesitic greenstone. Plain lines plot on the left-hand ordinate axis; dashed lines plot on the right hand ordinate axis. Data from [31]. Temperature is non-dimensionalized assuming $T_{sol} = 890°C$; $T_{liq} = 1170°C$; normalized using $\varphi = 0.5$.

processes in geological systems, and the results obtained are significant because they provide an insight into the processes by which granitic, tonalitic and granodioritic melt compositions may segregate from partially molten rock in the lower crust. These compositions correspond to only small fractions of equilibrium melting of the source rock [30–32]. The results presented in Sections 3.2 and 3.3 indicate that melt will segregate from a partially molten rock with suitable thermal and physical characteristics, while Fig. 6 allows an estimate of the time required for segregation. The results presented in Section 3.4 indicate that the composition of the segregated melt will correspond to a small fraction of equilibrium melting of the source rock.

The assumption that the pressures in the solid and liquid phases are equal, which leads to the equation governing conservation of linear momentum [equation (11)], is valid only if the matrix has no strength. This is equivalent to assuming that the matrix creep rate is rapid compared to matrix strain rate. Dimensional matrix strain rates predicted by the model are of the order $1/\tau$, where τ is the characteristic time; values of $1/\tau$ range from 10^{-20} to 10^{-30} s^{-1} for silicate rock phase change systems [equation (33)]. Data on liquid enhanced diffusional creep rates in silicate materials is limited; the results of deformation experiments on an olivine matrix saturated with basaltic liquid indicate that the diffusional creep rate in small (~ 10 μm) silicate grains, at porosities of ~ 0.08, must be rapid compared to the applied strain rate of $\sim 10^{-4}$ s^{-1} [18]. The equivalent stress on a liquid saturated matrix of 1 mm silicate grains, typical of rocks in the crust, would result in a strain rate of $\sim 10^{-10}$ s^{-1} [18, equation (2)]; this figure represents a best estimate of the maximum strain rate for which deformation by liquid enhanced diffusional creep in a partially molten silicate rock will satisfy the equal pressure approximation. Strain rates predicted by the model are 10–20 orders of magnitude less than this estimate, which indicates that the equal pressures approximation is robust.

Phase compositions may be specified because of the assumption of local thermodynamic equilibrium. Maintenance of equilibrium requires that the rate at which thermal and chemical equilibrium is attained is rapid compared to the thermodynamic evolution of the mixed phase region. Rates of thermal equilibration are rapid in both geological and metallurgical systems; the kinetic limit on the rate of chemical equilibration is species diffusion in the solid phase. The assumption of local thermodynamic equilibrium, therefore, limits the applicability of the model only to those systems in which diffusive rates are high, or thermodynamic evolution is slow. The high temperatures and extended duration of phase change in lower crustal melt zones suggests that the assumption of local thermodynamic equilibrium is justified in these systems, but it remains the most stringent limit on the general applicability of the model.

The results presented in this paper are intended to identify some of the generic features of a deformable mush undergoing solid–liquid phase change, to facilitate the development of more complex models. Future models will need to investigate the importance of thermal and compositional convection of the liquid phase, which causes decoupling of the solid and liquid phase velocities [25]. In the system discussed in this paper, the liquid is always at its solidus, and so its density is governed only by its composition; any change in

temperature causes a change in composition. Heating of the mush from below produces a stable compositional density gradient in the liquid for materials in which increasing degrees of equilibrium melting produce liquid of increasing density. This is the case for most silicate rocks. Hence, this simple analysis indicates that convection of the liquid phase is unlikely within partially molten rocks which are heated from below.

Future models will also need to investigate the possibility that fluid transport through a deformable matrix is an inherently 3-D problem. Wiggins and Speigelman [21] have developed solutions in 3-D to the problem of a buoyant liquid migrating through a deformable matrix, in the absence of phase change ($\Gamma_l = 0$), and in the limit of small background porosity. Their results indicate that an initially 1-D porosity wave will develop into groups of spherical, 3-D porosity waves. However, they placed no constraint on the vertical distance available for the development of 3-D waves. In our problem, a 1-D porosity wave forms only because the vertical extent of the mixed phase region is constrained by the position of the solidus isotherm; the upward rate of migration of the leading wave is primarily governed by the upward rate of migration of the solidus isotherm rather than the dynamics of the deformable mush. Furthermore, phase change due to pseudo-advection will act to inhibit the development of 3-D flow structures. In any region in which the upwards transport of liquid becomes focused, such as a chimney, the net phase velocity ($w_l + w_s$) increases, so the magnitude of the pseudo-advection term in equation (41) increases. This term acts to reduce the porosity, and hence permeability, consequently inhibiting liquid transport.

Acknowledgements—The authors would like to thank Michael Atherton for his inspiration, and two anonymous reviewers for their constructive comments. M.D.J. was supported by N.E.R.C. grant GT4/93/191/G.

REFERENCES

1. Bennon, W. D. and Incropera, F. P., A continuum model for the momentum, heat and species transport in binary solid–liquid phase change systems—I. Model formulation. *International Journal of Heat and Mass Transfer*, 1987, **30**, 2161–2170.
2. Loper, D. E. and Roberts, P. H., On the motion of an iron–alloy core containing a slurry. *Geophysical and Astrophysical Fluid Dynamics*, 1978, **9**, 298–321.
3. Hills, R. N., Loper, D. E. and Roberts, P. H., A thermodynamically consistent model of a mushy zone. *Quarterly Journal of Mechanics and Applied Mathematics*, 1983, **36**, 505–539.
4. Hills, R. N. and Roberts, P. H., On the formulation of diffusive mixture theories for two phase regions. *Journal of Engineering Mathematics*, 1988, **22**, 93–106.
5. Beckerman, C. and Viskanta, R., Natural convection solid/liquid phase change in porous media. *International Journal of Heat and Mass Transfer*, 1988, **31**, 35–46.
6. Clyne, T. W., Numerical modelling of directional solidification of metallic alloys. *Metal Science*, 1982, **6**, 441–450.
7. Viskanta, R., Heat transfer during melting and solidification of metals. *Journal of Heat Transfer*, 1988, **110**, 1205–1219.
8. Voller, V. R., Brent, A. D. and Prakash, C., The modelling of heat, mass and solute transport in solidification systems. *International Journal of Heat and Mass Transfer*, 1989, **32**, 1719–1731.
9. Bergantz, G. W., Conjugate solidification and melting in multicomponent open and closed systems. *International Journal of Heat and Mass Transfer*, 1992, **35**, 533–543.
10. Arzi, A. A., Critical phenomena in the rheology of partially melted rocks. *Tectonophysics*, 1978, **44**, 173–184.
11. van der Molen, I. and Paterson, M. S., Experimental deformation of partially melted granite. *Contributions to Mineralogy and Petrology*, 1979, **70**, 299–318.
12. Beere, W., A unifying theory of the stability of penetrating liquid phases and sintering pores. *Acta Metallica*, 1975, **23**, 131–138.
13. Bulau, J. R., Waff, H. S. and Tyburczy, J. A., Mechanical and thermodynamic constraints on fluid distribution in partial melts. *Journal of Geophysical Research*, 1979, **84**, 6102–6108.
14. Cheadle, M. J., Properties of texturally equilibrated two phase aggregates. Ph.D. thesis, University of Cambridge, Cambridge, U.K., 1989.
15. Bennon, W. D. and Incropera, F. P., A continuum model for the momentum, heat and species transport in binary solid–liquid phase change systems—II. Application to solidification in a rectangular cavity. *International Journal of Heat and Mass Transfer*, 1987, **30**, 2171–2187.
16. Pharr, G. M. and Ashby, M. F., On creep enhanced by a liquid phase. *Acta Metallica*, 1983, **31**, 129–138.
17. Cooper, R. F. and Kohlstedt, D. L., Solution–precipitation enhanced diffusional creep of partially molten olivine–basalt aggregated during hot pressing. *Tectonophysics*, 1984, **107**, 207–233.
18. Kohlstedt, D. L. and Chopra, P. N., Influence of basaltic melt on the creep of polycrystalline olivine under hydrous conditions. In *Magmatic Systems*, 1st edn, ed. M. P. Ryan. Academic Press, San Diego, 1994, chapter 3.
19. McKenzie, D., The generation and compaction of partially molten rock. *Journal of Petrology*, 1984, **25**, 713–765.
20. Richter, F. M. and McKenzie, D., Dynamical models for melt segregation from a deformable matrix. *Journal of Geology*, 1984, **92**, 729–740.
21. Barcilon, V. and Richter, F. M., Nonlinear waves in compacting media. *Journal of Fluid Mechanics*, 1986, **164**, 429–448.
22. Wiggins, C. and Spiegelman, M., Magma migration and magmatic solitary waves in 3-D. *Geophysical Research Letters*, 1995, **22**, 1289–1292.
23. Huppert, H. E. and Sparks, R. S. J., The generation of granitic magmas by intrusion of basalt into continental crust. *Journal of Petrology*, 1988, **29**, 599–624.
24. Bergantz, G. W. and Dawes, R., Aspects of magma generation and ascent in continental lithosphere. In *Magmatic Systems*, 1st edn, ed. M. P. Ryan. Academic Press, San Diego, 1994, chapter 13.
25. Lowell, R. O. and Bergantz, G. W., Melt stability and compaction in a partially molten silicate layer heated from below. In *Structure and Dynamics of Partially Solidified Systems*, ed. D. E. Loper. Nato ASI Series, Series E, Vol. 125, Martinus Nijhoff, 1987, pp. 385–400.
26. Prescott, P. J., Incropera, F. P. and Bennon, W. D., Modelling of dendritic solidification systems: reassessment of the continuum momentum equation. *International Journal of Heat and Mass Transfer*, 1991, **34**, 2351–2359.
27. Landau, L. D. and Lifshitz, E. M., *Fluid Mechanics*, 1st edn. Pergamon Press, London, 1959, p. 536.
28. Scott, D. and Stevenson, D., Magma ascent by porous flow. *Journal of Geophysical Research*, 1986, **91**, 9283–9296.

29. Bear, J., *Dynamics of Fluids in Porous Media*, 1st edn. Elsevier, New York, 1972, p. 764.
30. Patino Douce, A. E. and Johnston, A. D., Phase equilibria and melt productivity in the pelitic system: implications for the origin of peraluminous granitoids and aluminous granulites. *Contributions to Mineralogy and Petrology*, 1991, **107**, 202–218.
31. Beard, J. S. and Lofgren, G. E., Dehydration melting and water-saturated melting of basaltic and andesitic greenstones and amphibolites at 1, 3 and 6.9 kb. *Journal of Petrology*, 1991, **32**, 365–401.
32. Rapp, R. P. and Watson, E. B., Dehydration melting of metabasalt at 8–32 kbar: implications for continental growth and crust-mantle recycling. *Journal of Petrology*, 1995, **36**, 891–931.
33. Carslaw, H. S. and Jaeger, J. C., *Conduction of Heat in Solids*, 2nd edn. Clarendon Press, Oxford, U.K., 1986, p. 510.
34. Morton, K. F. and Mayers, D. F., *Numerical Solution of Partial Differential Equations*, 1st edn. Cambridge University Press, Cambridge, U.K., 1994, p. 228.
35. Press, W. H., Teukolsky, S. A., Vetterling, W. T. and Flannery, B. P., *Numerical Recipes in Fortran*, 2nd edn. Cambridge University Press, Cambridge, U.K., 1992, p. 934.
36. Siemieniuch, J. L. and Gladwell, I., Analysis of explicit difference methods for a diffusion–convection equation. *International Journal of Numerical Methods in Engineering*, 1978, **12**, 899–916.